

Characterization of a High Specific Impulse Xenon Hall Effect Thruster

IEPC-2005-324

Presented at the 29th International Electric Propulsion Conference, Princeton University,
October 31 – November 4, 2005

James J. Szabo*
Busek Co. Inc, Natick, MA, 01760, USA

Yassir Azziz†
MIT, Cambridge, MA, 02139, USA

A high specific impulse Hall Effect Thruster was developed and characterized with xenon propellant. Such a thruster may be used for interplanetary missions as well as satellite orbit raising and repositioning. The thruster has a dielectric discharge channel and is scaled for operation at power levels up to several kW. At 1 kV, 2.3 kW, the anode specific impulse is 3200 s, the thrust efficiency is 52%, and the beam divergence is 35°. The maximum measured thrust efficiency is 60%. The maximum measured specific impulse is >3400 s. The thruster is also capable of throttling to low I_{sp} operating points while maintaining efficiencies above 50%. This work showed that Hall Effect Thrusters can compete with ion engines for applications at several kW.

I. Nomenclature

A_e	=	exit area of discharge channel
\vec{B}	=	magnetic field
B_{min}	=	magnetic field magnitude required to minimize the discharge current
\vec{D}	=	mid-channel diameter
\vec{E}	=	electric field
g_0	=	gravitational constant at Earth's surface, 9.81 m/s ²
I_b	=	beam current
I	=	current, subscripts b for beam, d for discharge, s for solenoids
I_{sp}	=	specific impulse (effective exhaust velocity divided by g)
j	=	current density
k	=	Boltzmann constant
m	=	mass of an electron
\dot{m}	=	mass flow rate, subscripts a for anode, b for backflow.
M	=	mass of Xe ion (131 amu)
n	=	density, subscripts e for electron, I for ion, n for neutral.
P_d	=	discharge power
Q_{in}	=	cross section for reaction $e + Xe \rightarrow 2e + Xe^+$
R	=	radial dimension

* Research Scientist, jszabo@busek.com.

† Graduate Student, Department of Aeronautics and Astronautics, yazziz@mit.edu.

T	=	thrust; temperature
v_n	=	neutral velocity
V_d	=	discharge power supply voltage (between floating cathode and anode)
Z	=	axial dimension; degree of ionization
β	=	Hall parameter
η_t	=	thrust efficiency
θ	=	angular dimension

II. Introduction

IN a Phase II SBIR program sponsored by NASA, Busek Co. Inc. built a 2.3 kW laboratory model Hall thruster with a nominal specific impulse of 3200 seconds, similar to the highest power NSTAR ion engine requirement.¹ This laboratory model thruster, called the BHT-1500, was delivered to NASA GRC in 2004. This paper describes experimental characterization of the thruster, including thrust and plume measurements. It also describes related numerical modeling.

A. Hall Effect Thrusters

The working fluid of a Hall Effect Thruster (HET) is plasma and the means of acceleration is an electric field. The plasma is created inside a channel, which is usually annular and can be dielectric or metallic. Usually, an electric potential is applied between a gas distributor located at the base of the channel and a cathode located outside the channel. This creates an axial electric field. The current between the cathode and anode is impeded by an orthogonal magnetic field. Instead of traveling directly to the anode, electrons drift azimuthally due to the $\vec{E} \times \vec{B}$ Hall Effect, allowing them time to collision-ionize the gas. Since ions are only weakly affected by the magnetic field, most are accelerated out of the channel, forming an ion beam. Cathode electrons neutralize the ion beam. Because the plasma in the discharge channel is quasi-neutral, no space charge limitation arises, allowing HETs to operate at higher number densities than ion engines.

HETs were originally developed in the United States in the 1960s.² By the end of 1962, annular thrusters had been tested at NASA Lewis Research Center,^{3,4} Avco,⁵ and United Aircraft Corporation Research Laboratories.^{5,6,7} Noble gas thrusters were well developed by the mid-sixties.⁸ In the US, research waned around 1970; gridded ion engines were more efficient in the high I_{sp} range of interest at the time.² However, work continued in the Soviet Union, where the Hall thruster was developed into a practical device for satellite station-keeping in the 1970s and 1980s.⁹ Soviet contributions included the identification of magnetic design criteria promoting both stability and efficiency.^{10, 11} Western interest was renewed in the early 1990s when the extent of Soviet success was well publicized.¹² American thrusters soon followed.¹³

Busek Co. Inc. has been building HETs since the mid-1990s. Our thrusters range in power from hundreds of watts to tens of kilowatts. We have experience with a wide variety of propellants, including xenon, krypton, bismuth, and even air.

B. Performance Parameters

The thrust produced by a HET is a function of the neutral mass flow rate, the degree to which the neutrals are ionized, the fraction of ions that survive to enter the beam, the amount of energy imparted to these ions, and the beam divergence. The effective exhaust velocity is the thrust divided by the mass flow rate. Normalizing by g_0 , the acceleration of gravity, yields the specific impulse or I_{sp} .

The efficiency of the discharge may be assessed with the expression $\eta_t = T^2 / 2\dot{m}_a I_a V_d$, known as the thrust efficiency. Here T is thrust, I_a is anode current, V_d is discharge voltage, and \dot{m}_a is the mass flow rate of neutrals to the anode. The discharge power is $P_d = I_a V_d$. One can express the thrust efficiency as the product of the acceleration, utilization, and electrical efficiencies, divided by the mean charge of the ions.

C. The BHT-1500

The BHT-1500 is a single stage laboratory model HET suitable for high voltage plasma discharges up to several kW in power. The discharge channel is lined with boron nitride. This material was chosen for its thermal stability, high temperature dielectric strength, and low sputter yield. As delivered to NASA GRC, the BHT-1500 was

equipped with a Busek hollow cathode and a Busek propellant voltage isolator. Figure 1 shows the thruster so equipped and a plume generated at the design point of $P_d=2.3$ kW, $V_d=1000$ V, anode $I_{sp}=3200$ s.

The magnetic circuit was optimized for $|B| > 500$ Gauss in the channel, required for $P_d=2.3$ kW, $V_d=1000$ V. The anode assembly passively shunts a portion of the magnetic field, creating a magnetic lens with a sharp drop in $|B|$ close the anode.¹⁴ This results in a desirable electric potential distribution.

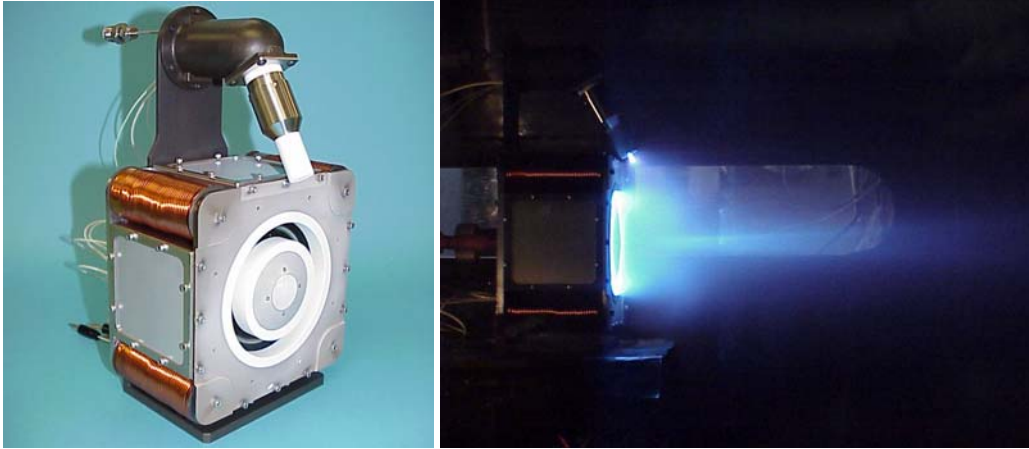


Figure 1. Left: BHT-1500. Right: Plume at 2.3 kW, 1000 V.

III. Test Facilities

The BHT-1500 was tested in the vacuum chamber shown in Figure 2. This facility can theoretically pump 180,000 liters/second of xenon, resulting in pressures near or below 1×10^{-5} Torr for the tests reported here.

Performance was measured with a thrust stand of the inverted pendulum type originally developed at NASA Glenn Research Center.^{15,16} With this type of stand, thrust is proportional to the displacement of a platform on which the thruster is mounted. In our stand, displacement is measured with a Schaevitz 050 HR Linear Variable Differential Transformer (LVDT). The voltage signal is read into a computer data acquisition card so that it can be filtered and monitored using a National Instruments LabView program. The thrust stand is calibrated at the beginning of each test.

The discharge was powered by a Universal Voltronics BRC 10,000 power supply. Xenon mass rates were regulated by Unit Instruments model UFC 7300 flow controllers.



Figure 2. Busek's 8-ft. diameter, 18-ft. long vacuum test facility

- Stainless Steel, 2.4 m x 5 m Long
- Single and two-Stage Cryo-pumps
 - 180,000 l/s
- NASA GRC Type Thrust Stand
- Automated data acquisition
- Automated probe positioner
 - Variable R, theta
- Plume Diagnostics
 - Faraday probe
 - Retarding Potential Analyzer
 - Langmuir probe
 - Emissive probes
 - Optical and IR Spectroscopy

The test facility is equipped with an automated probe positioner featuring an extendable rotating arm, as shown in Figure 3. A maximum of 180° of rotation is accomplished through a Danaher Precision Systems RTR-6 rotary stage. The positioner is also equipped with a Danaher custom linear stage with 24 inches of extension that controls

the sweep radius. Empire Magnetics vacuum rated stepper motors (model U22-VC) drive each stage. The pivot axis is positioned below the exit plane of the thruster. The vertical height of the probe is set to bisect the plume, passing through its axis. Data acquisition is highly automated. A LabView program controls the positioner and collects the data. The LabView program commands a Galil DMC-2123 2-axis Ethernet based motion controller with an ICM-20105 opto-isolated I/O module. The Galil controller commands stepper motor drivers (Applied Motion Products, model 3540 M). Prior to data collection, the user specifies the sweep radius, the boundaries of the angular rotation, and the increment of the angular rotation. Other variables include dwell (settling) time before taking data after the arm is moved and the number of samples to be taken at each position.

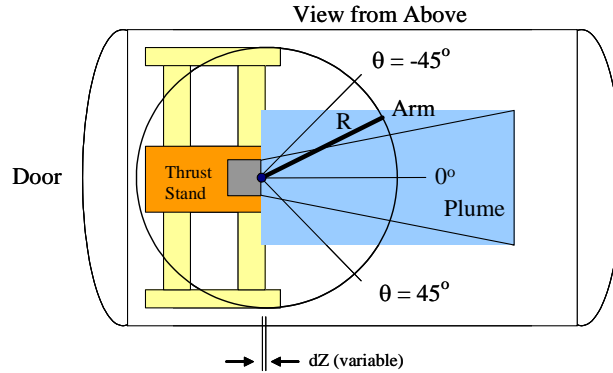


Figure 3. Diagram of probe positioner.

IV. Experimental Results

The first section of experimental results surveys performance in the range $300 \leq V_d \leq 1000$ and $2.4 \leq \dot{m}_a \leq 4.9$ mg/s. The second section takes a more detailed look at $\dot{m}_a = 2.4$ mg/s, the flow rate required for $I_{sp} = 3200$ s at $P_d = 2.3$ kW, $V_d = 1000$ V. The third section describes plume current measurements at $\dot{m}_a = 2.4$ mg/s, $V_d = 1000$ V. The final section presents numerical predictions of discharge properties at $\dot{m}_a = 2.4$ mg/s, $V_d = 1000$ V.

A. Performance Survey

Thrust was measured at a variety of flow rates and discharge voltages. This section presents results of a comprehensive survey conducted in the ranges $300 \leq V_d \leq 1000$ V and $2.4 \leq \dot{m}_a \leq 4.9$ mg/s.

The appendix quantifies error bars in thrust and associated figures of merit. It also explains a correction we applied to account for neutrals flowing from the test facility back into the discharge.

Figure 4 plots thrust efficiency vs. discharge power. The two parameters are clearly correlated. The thrust efficiency is about 60% at $P_d = 3$ kW and $>50\%$ when $P_d > 1500$ W. Although the thrust efficiency does not appear to reach an asymptotic maximum at 3 kW, we capped the discharge power to avoid potentially damaging the thruster.

Figure 5 plots thrust efficiency vs. discharge potential, V_d . The highest efficiency plotted is $\eta_t = 59\%$, at $V_d = 650$ V, $P_d = 2.9$ kW, $\dot{m}_a = 4.9$ mg/s, anode $I_{sp} = 2710$ s. The thruster has been characterized up to $V_d = 1200$ V (results reported in next section). However, it has not yet been characterized at $V_d < 300$ V or $\dot{m}_a > 4.9$ mg/s.

Figure 6 plots anode I_{sp} vs. V_d . Propellant utilization appears to increase with V_d and/or P_d . If propellant utilization were constant, we would see $I_{sp} \sim \sqrt{V_d} \sim \sqrt{P_d}$. Experimentally, I_{sp} rises at a faster rate.

The method used to optimize the magnetic field can greatly affect the thrust efficiency at some operating points (\dot{m}_a, V_d). The discharge is coarsely tuned by varying the magnitude of the solenoid current, I_s , to minimize the discharge current. Let us call the magnitude of \vec{B} at this point B_{min} . Sometimes, the discharge may be finely tuned to decrease discharge current oscillations by deviating from B_{min} . Statistically significant efficiency improvements have been observed at some of these fine tuned points.

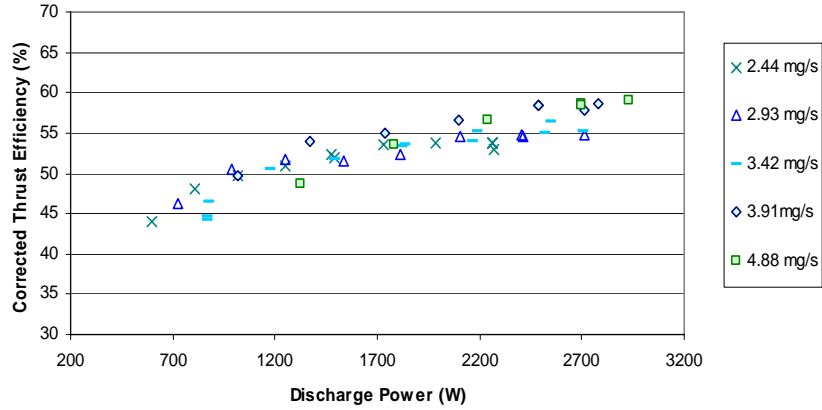


Figure 4. Thrust efficiency vs. discharge power for five mass flow rates.

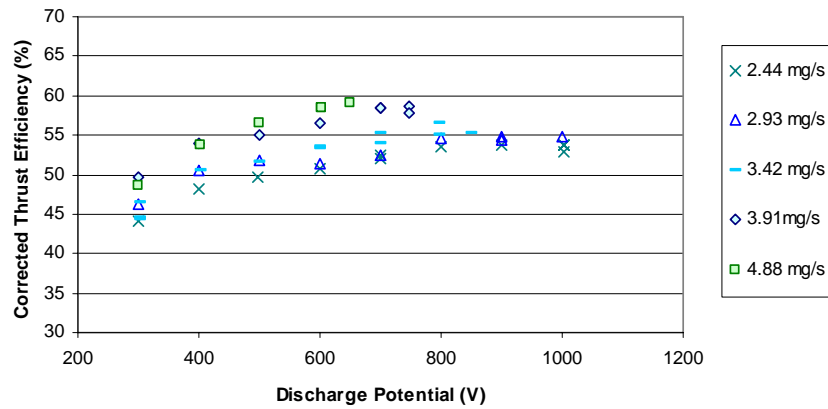


Figure 5. Thrust efficiency vs. discharge voltage (potential) for five mass flow rates.

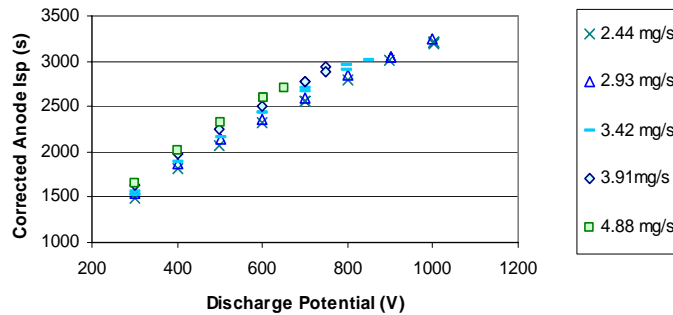


Figure 6. Anode I_{sp} vs. discharge voltage (potential) for five mass flow rates.

Experimental data plotted in Figure 7 show that B_{min} increases roughly in proportion to V_d when the voltage is varied at $\dot{m}_a = 2.44$ mg/s. To make this plot, we correlated the current through the solenoids, I_s , during testing at $300 \leq V_d \leq 1000$ with bench-top measurements of $|B|$ in the exit plane of the thruster. We assume that operational

temperatures do not appreciably effect $|B|=fn(I_s)$. Numerical modeling of MIT's mini-TAL also showed that B_{min} increases in proportion to voltage.¹⁷

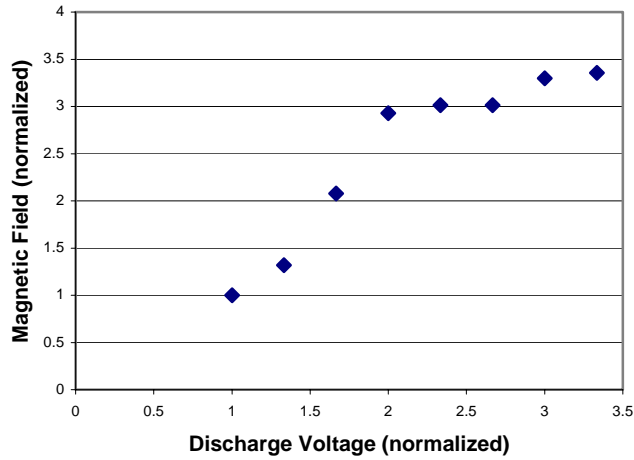


Figure 7. Normalized $|B|$ for minimum discharge current vs. normalized discharge voltage from $V_d=300$ V to $V_d=1000$ V. An Ion Tech hollow cathode was used when these data were taken.

B. Acceptance Test

This section describes the final test conducted before we shipped the thruster to NASA GRC. The data provide a detailed look at $\dot{m}_a=2.4$ mg/s, the flow rate required for $I_{sp}=3200$ s at $P_d=2.3$ kW. The test conditions and data are listed in Table 1. Thrust was first measured at $300 \leq V_d \leq 1000$ Volts at $\dot{m}_a = 2.4$ mg/s. Thrust was next measured at $300 \leq V_d \leq 800$ Volts and $\dot{m}_a = 4.0$ mg/s. Finally, thrust was measured at $1100 \leq V_d \leq 1200$ Volts at $\dot{m}_a = 2.4$ mg/s. The test was conducted with a $40 \mu F$ capacitor bank across the discharge power supply. The cathode mass flow rate was 10% of the total flow rate, although less cathode flow is required.

Table 1. Acceptance test data. Cathode heater current = 3 A. Cathode keeper current = 0.5 A. Discharge current minimized.

Anode Discharge Voltage (V)	Anode Discharge Current (A)	Solenoid Current (A)	Cathode Floating Voltage (V)	Tank Pressure [Torr]	Xe Anode Flow (mg/s)	Xe Cathode Flow (mg/s)	Thrust (mN)	Est. Neutral Backflow Correction (mg/s)	Corrected Thrust Efficiency (%)	S.D. Thrust Efficiency p/m (%)	Corrected Anode Isp (s)	S.D. Anode Isp p/m (s)
300	1.98	2.1	-17.1	7.3E-06	2.44	0.276	35.6	0.009	43.6	2.3	1483	41
400	2.04	2.5	-17.06	7.0E-06	2.44	0.276	43.3	0.008	46.8	2.2	1800	45
501	2.11	3.8	-17.8	7.2E-06	2.44	0.276	49.3	0.009	46.9	2.1	2050	48
501	2.11	3.8	-17.7	7.3E-06	2.44	0.276	49.3	0.009	46.9	2.0	2051	46
600	2.19	4.7	-18.9	7.3E-06	2.44	0.276	55.8	0.009	48.3	1.9	2321	49
700	2.22	5.6	-19.3	7.3E-06	2.44	0.276	62.2	0.009	50.8	1.8	2589	51
800	2.25	10.1	-20	7.3E-06	2.44	0.276	66.6	0.009	50.3	1.8	2772	53
799	2.24	9.8	-20.2	7.4E-06	2.44	0.276	67.4	0.009	51.8	1.8	2806	53
900	2.27	9.0	-19.5	7.3E-06	2.44	0.276	72.7	0.009	52.9	1.8	3027	56
1002	2.31	7.8	-19.4	7.4E-06	2.44	0.276	77.2	0.009	52.6	1.7	3213	58
1002	2.34	6.1	-18.8	7.8E-06	2.44	0.276	77.0	0.009	51.6	1.7	3204	58
1002	2.36	7.1	-17.4	7.7E-06	2.44	0.345	77.1	0.009	51.3	1.7	3209	58
300	2.02	1.7	-15.7	7.4E-06	2.44	0.345	36.3	0.009	44.4	2.3	1511	40
300	3.42	2.4	-16	1.0E-05	3.91	0.414	63.8	0.012	50.7	1.8	1660	32
400	3.44	3.0	-16.4	1.0E-05	3.91	0.414	77.0	0.012	55.0	1.8	2004	36
500	3.53	4.6	-17.7	1.0E-05	3.91	0.414	87.6	0.012	55.5	1.7	2279	40
599	3.59	4.9	-17.9	1.0E-05	3.91	0.414	98.4	0.013	57.4	1.7	2560	43
700	3.66	5.3	-17.9	1.1E-05	3.91	0.414	108.5	0.013	58.7	1.7	2823	47
799	3.73	7.3	-18.7	1.1E-05	3.91	0.414	117.0	0.013	58.6	1.7	3044	49
799	3.77	4.8	-17	1.1E-05	3.91	0.414	118.8	0.013	59.8	1.7	3092	50
1103	2.32	6.1	-18.8	8.3E-06	2.44	0.276	81.0	0.010	52.3	1.7	3368	60
1199	2.36	8.0	-17.07	8.3E-06	2.44	0.276	81.9	0.010	48.3	1.6	3406	62
1199	2.36	6.9	-17.9	8.4E-06	2.44	0.276	82.2	0.010	48.8	1.6	3420	63

Like Figure 7, the data in Table 1 at $V_d \leq 700$ V show B_{min} (proportional to I_s below $I_s=7$ A) increasing in proportion to V_d . The data are scattered at higher voltages.

Figure 8 plots η_t with error bars. Figure 9 plots anode I_{sp} with error bars. Thrust efficiency was between 51.3% and 52.6% near the design point of $V_d=1000$ V, $P_d=2.3$ kW, anode $I_{sp}=3200$ s. Efficiency dropped at above 1 kV. At $V_d=1100$ V and $P_d=2.6$ kW, we measured $\eta_t=52.3\%$ and anode $I_{sp}=3368$ s. At 4.0 mg/s, $V_d=799$ V and $P_d=3.1$ kW, we measured $\eta_t=59.8\%$ and anode $I_{sp}=3092$ s. This may be the most favorable operating point. At $P_d=1$ kW and $\dot{m}_a = 4.0$ mg/s, we measured $\eta_t=50.7\%$ and anode $I_{sp}=1660$ s

Error bars ($\pm \sigma$) were calculated according to the methodology outlined in the appendix. The normalized thrust efficiency error is 3.3% at the design point ($I_{sp}=3200$ s, $P_d=2.3$ kW). In absolute terms, the error is $\pm 1.7\%$. The normalized I_{sp} error is about 1.8% (± 58 s) at the design point. The mass flow rates used to calculate η_t and anode I_{sp} are corrected for neutral backflow from the test chamber, but the correction is small (the decrease in efficiency is 0.1%-0.2%) because the maximum tank pressure was quite modest.

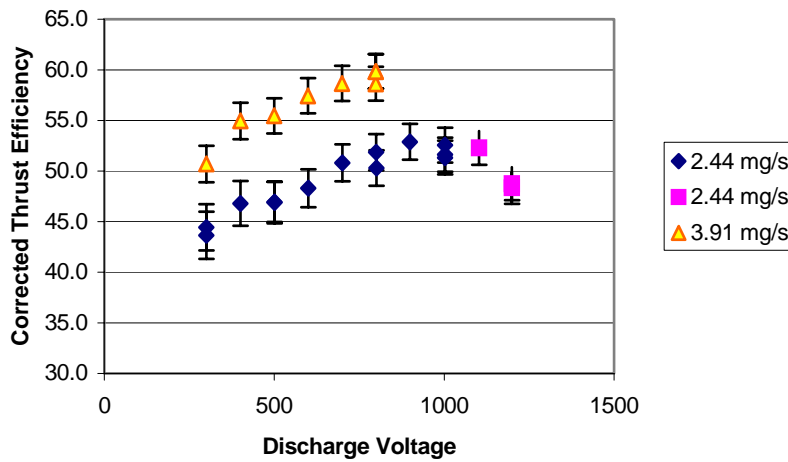


Figure 8. Acceptance test thrust efficiency with error bars.

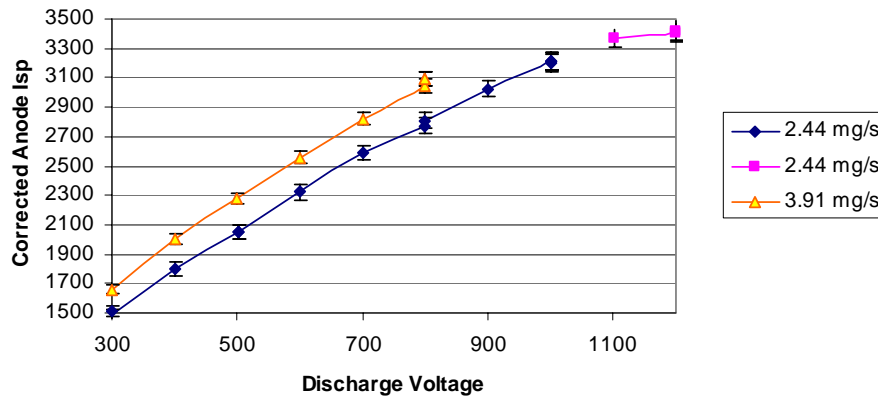


Figure 9. Acceptance test specific impulse with error bars.

C. Plume Measurements

Current density was measured with a nude Faraday probe originally developed at MIT.^{18,19} The current density was extrapolated to in-orbit conditions to determine plume divergence at $V_d=1000$ V, the voltage required for $I_{sp}=3200$ s at $P_d=2.3$ kW and $\dot{m}_a=2.4$ mg/s.

The probe, shown in Figure 10, consists of a 0.175 inch collector enclosed in a 0.25 inch guard ring that shields the collector from low energy ions. The gap between the collector and the guard ring is designed to allow a smooth sheath surface over the collector. The collector and guard ring are both made of stainless steel and are normally biased to -20 V to repel electrons. The Faraday probe has been cross-calibrated against a larger and well-characterized JPL probe at the University of Michigan's Plasmadynamics and Electric Propulsion Laboratory.²⁰ The results of the cross-calibrations show good agreement between data obtained from both probes. A detailed discussion of the results can be found in previous publications.^{18, 19}

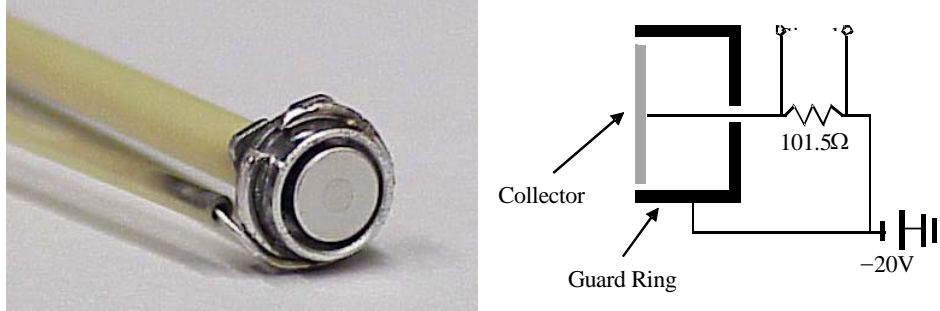


Figure 10. Left: Picture of the Faraday probe. Right: Electrical diagram of the Faraday probe.

Collected current is determined by measuring the voltage drop across a 101.5Ω resistor, as shown in Figure 10. The voltage drop is acquired by a 22-bit HP34970A Agilent Data Logger, and is then stored in a file created by the same LabView program that commands the plume positioner. A Faraday sweep performed in 1° increments takes approximately 20 minutes. The thruster is usually run for 1-2 hours before plume measurements are taken to allow the discharge chamber walls to outgas and reach a thermal steady state.²¹ The cathode is allowed to float, and usually hovers between 15 and 20 V below the facility ground.

For these measurements, the Faraday probe was placed 1 meter downstream the exit plane of the thruster. The xenon flow rate was 2.44 mg/s to the anode and 0.25 mg/s to the cathode. The background pressure was approximately 6×10^{-6} Torr. A $40 \mu\text{F}$ capacitor was placed in parallel with the discharge power supply to minimize discharge voltage oscillations. The solenoid current was adjusted to minimize the discharge current.

Figure 11 plots current density for the BHT-1500 plume at $V_d=300$ V, 600 V and 1000 V. As reported previously,²² plume divergence decreases as the anode voltage increases.

For $V_d = 1000\text{V}$, the half-angle plume divergence angle is 35 degrees.[‡] This angle is based on 95% of the beam current and was calculated using the following equation:

$$0.95I_b = 2\pi r^2 \int_0^{\theta_d} j(\theta) \sin \theta d\theta. \quad (1)$$

Here, I_b is the beam current, r is the sweep radius, j is the current density, θ is the probe's angular position, and θ_d is the divergence angle. Before calculating the divergence angle, tank effects were excluded from $j(\theta)$. According to an established methodology,²³ we extended the exponential portion of $j(\theta)$ between 10° and 30° to $\pm 90^\circ$.

[‡] A detailed discussion of discharge voltage effects on plume current density for a different configuration of the BHT-1500 can be found in Ref. 22

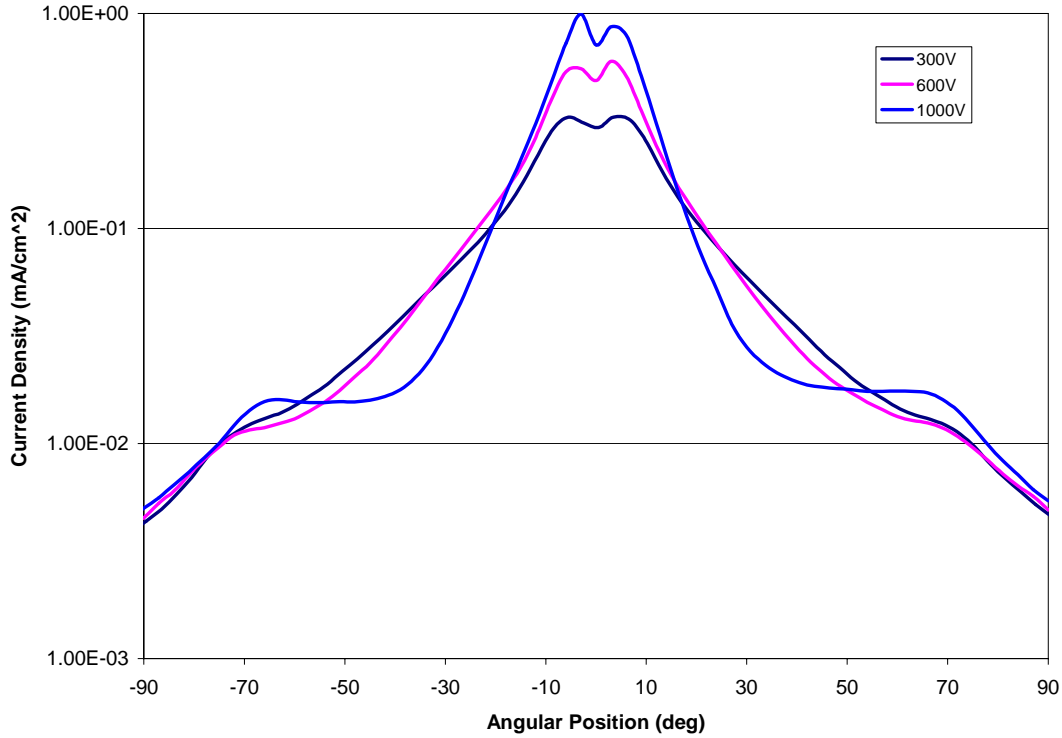


Figure 11. Current density profiles versus angular position at $V_d = 300\text{V}$, 600V and 1000V .

D. Numerical Modeling

We also studied the $V_d=1000$ V discharge with a 2D-3V full Particle-In-Cell (PIC) Monte Carlo Collision (MCC) numerical simulation.²⁴ The numerical results give insight into the properties of the plume. Past work with the BHT-1000, a slightly smaller thruster which preceded the BHT-1500, showed that the simulation does a reasonable job of predicting plasma properties in and near the channel.²¹

The full PIC code models all species as particles. The electric field is determined by solving Poisson's equation for the electric potential starting from the charge distribution and boundary conditions. Most collisions are modeled using the MCC methodology, which is appropriate for unlike particles (e.g. electrons and neutrals). We imposed a numerical hall parameter of $\beta=200$ everywhere. Normally, at the beginning of the simulation, the channel is allowed to fill with neutrals without an electrical discharge present. The channel is then seeded with plasma. The solution is then converged until it reaches a state of quasi-equilibrium, characterized by repeatable oscillations in the discharge current. To generate the results reported here, we started from a previously converged solution.

The magnetic field was pre-calculated assuming a solenoid current of $I_s=5$ A. In the laboratory, stable $V_d=1000$ V discharges at $\dot{m}_a=2.44$ mg/s were achieved with I_s between 6 and 8 Amps. Therefore, we multiplied the calculated magnetic field strength by a factor of 1.5.

As in previous work when the hall parameter was fixed,²¹ the propellant utilization was under-predicted. Experimentally, $V_d=1000$ V and $\dot{m}_a=2.44$ mg/s yields $I_{sp}=3200$ s at $P_d=2.3$ kW, $\eta_t=52\%$. The simulation only predicted $I_{sp}=2740$ s at $P_d=1.7$ kW, $\eta_t=52\%$. We believe a more realistic electron diffusion model is required. Nevertheless, plasma properties lend insight into the discharge.

Figure 12 (left) shows the computational grid used to solve for the electric potential, ϕ , and apply it to the particles. Figure 12 (right) shows calculated electric potentials. Approximately 20% of the total potential drop occurs outside the channel, where the resulting electric field is divergent.

Figure 13 (left) plots the ion number density with streamlines of \vec{E} . Inside the channel, \vec{E} is largely axial. However, the ion beam is canted slightly toward the thruster's axis. If ions continue on the path shown, the focal

point of the beam will be about 1 meter in front of the thruster. Some ions created near the inner channel wall may not survive to enter the beam. Others will enter the beam with a significant radial velocity component due to radial components of \vec{E} . Figure 13 (right) plots the number density of ions created through the charge exchange process with streamlines of \vec{E} . Ions created near the exit of the channel through electron impact or charge exchange may enter the beam with a strong radial velocity component.

The electric potential, electric field, and ion densities plotted here were obtained time averaging across an ionization oscillation cycle.

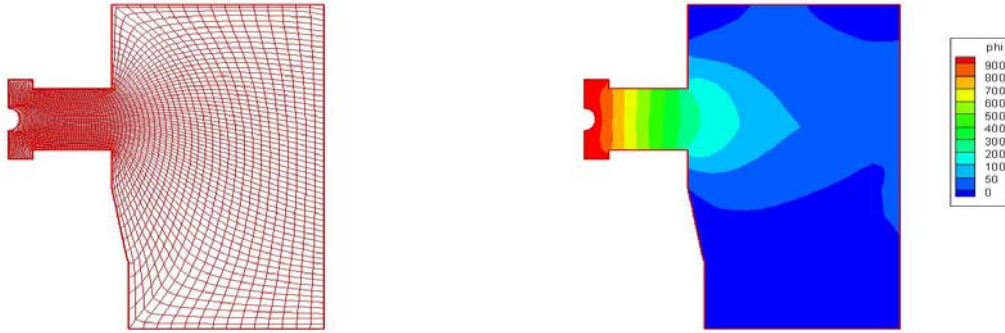


Figure 12. Left: Computational grid for BHT-1500. Right: Electric potentials (V) for BHT-1500 at 1000 V. Not to scale.

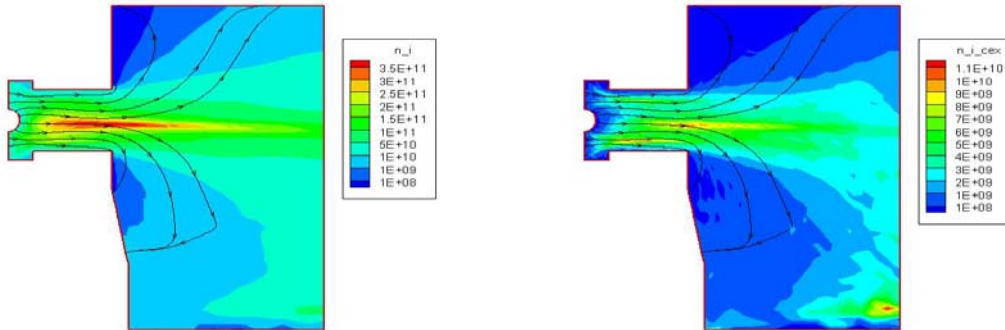


Figure 13. Ion density ($1/\text{cm}^3$) with streamlines of \vec{E} . Left: Total ion number density. Right: Ions produced through charge exchange process only. Not to scale.

V. Discussion

It is uncertain how high the exhaust velocity can ultimately be pushed. However, it is clear from this program that $I_{sp}=3000$ s is both possible and practical for 2-3 kW Hall Effect Thrusters.

The most direct way to increase the efficiency at high I_{sp} is operate closer to the ideal scaling curve.²⁵ Ideal scaling laws say that the discharge power should be proportional to the mean channel diameter, $P \sim D$. If other dimensions scale linearly, then the surface area of the thruster scales as $A \sim D^2$. If the waste heat to be radiated is proportional to the total discharge power, then the thermal equilibrium temperature is an inverse function of mean diameter, $T \sim (1/D)^4$. To keep temperatures modest at both high voltage and small D , the mass flow rate must be decreased below the value which maximizes propellant utilization. Without substantially altering the discharge channel dimensions or physics, we may reduce T by adding radiators and thermal shunts. This may allow long lifetime at $P > 3$ kW.

Another way to improve performance is to use numerical tools like the full PIC code to decrease radial electric field components which drive ions into the wall, decreasing propellant utilization, and increase plume divergence, decreasing the acceleration efficiency. Wall losses also drive T, which constrains the plasma density at high voltage.

Alternate propellants such as bismuth may also yield better high I_{sp} performance than xenon at modest power levels.

VI. Conclusions

Busek showed that is technically feasible to compete with ion engines using Hall Effect Thrusters for applications at the several kilowatt power level. The BHT-1500 demonstrated the ability to operate at greater than 50% thrust efficiency at $P_d=2.3$ kW, anode $I_{sp}=3200$ s. The beam divergence is 35° at this point. The maximum thrust efficiency is 60%, obtained at slightly lower I_{sp} and slightly greater power. The thruster is also capable of throttling to relatively low I_{sp} operating points while maintaining thrust efficiencies of about 50%.

Appendix: Error Analysis

This section explains the error bars for thrust efficiency and specific impulse. In general, for a function $y=F(X_1, X_2, X_n)$, small variations in x_i will alter y according to:²⁶

$$dy = \sum_{i=1}^n \frac{\partial F}{\partial x_i} dx_i .$$

The variance, σ_i^2 of the i th component is then

$$\sigma^2 = \sum_{i=1}^n \left(\frac{\partial F}{\partial x_i} \right)^2 \sigma_i^2 .$$

For thrust efficiency, $\eta_t = T^2/2\dot{m}P_d$, the normalized variance is

$$\left(\frac{\sigma_\eta}{\eta} \right)^2 = 4 \left(\frac{\sigma_T}{T} \right)^2 + \left(\frac{\sigma_{\dot{m}}}{\dot{m}} \right)^2 + \left(\frac{\sigma_{P_d}}{P_d} \right)^2 .$$

For specific impulse, $I_{sp}=T/\dot{m}$, the variance is

$$\left(\frac{\sigma_{I_{sp}}}{I_{sp}} \right)^2 = \left(\frac{\sigma_T}{T} \right)^2 + \left(\frac{\sigma_{\dot{m}}}{\dot{m}} \right)^2 .$$

The error bars on the graphs in this paper show one standard deviation, σ_i .

Table 2 quantifies the most significant sources of error in the efficiency and I_{sp} calculations.

Table 2. Typical errors for BHT-1500 testing

Power	Voltage	0.05
	Current	1
	Standard Dev. (RMS)	1.0
Mass Flow	Controller (99.2%)	1
	Backflow (0.8%)	1
	Standard Dev. (RMS)	1.0
Thrust	Slope of calibration curve	1
	LVDT signal (.12 V)	1.67
	Standard Dev. (RMS)	1.9
Efficiency	Standard Dev. (RMS)	4.1
Isp	Standard Dev. (RMS)	2.2

The error in the LVDT signal accounts for thermal drift of the thrust stand and other factors. Neutral backflow into the thruster was estimated with the equation

$$\dot{m}_{bf} = n_n M \langle v_x \rangle A_e,$$

where $\langle v_x \rangle = \sqrt{kT/2\pi M}$ and $n_n = P/kT$. A background temperature of 300 K was assumed. We assumed 100% uncertainty in this correction, i.e. $(\sigma_{\dot{m}_{bf}}/\dot{m}_{bf})^2 = 1.0$.

Acknowledgments

This work was funded under NASA Contract No. NAS3-01124, monitored by David Jacobson. Personnel at or associated with Busek who contributed to this project include James Szabo, Bruce Pote, Vlad Hruby, Seth McElhinney, Peter Rostler, Juraj Kolencik, Henry Neeser, Rachel Tedrake, Larry Byrne, Walt Pearlman, Julio Cordero, Tim Pidgeon, Chas Freeman, Josef Miklicek, Melissa Lowe, and Judy Budny. Busek also wishes to acknowledge the contributions by MIT Professor Manuel Martinez-Sanchez.

References

- 1 T. Bond, G. Benson, J. Christensen, J. Gallagher, M. Matranga, "The NSTAR Ion Propulsion Subsystem for DS1," AIAA-99-2972.
- 2 H. R. Kaufman, "Technology of Closed-Drift Thrusters," *AIAA Journal*, Vol. 23, No. 1, 1985. pp. 78-87.
- 3 G. R. Seikel and E. Reshotko, "Hall Current Ion Accelerator," *Bulletin of the American Physical Society*, Ser. II, Vol. 7, June 1962, p. 414.
- 4 G. R. Seikel, "Generation of Thrust – Electromagnetic Thrusters," *Proceedings of the NASA-University Conference on the Science and Technology of Space Exploration*, Vol. 2, Nov. 1962, pp. 171-176.
- 5 M. C. Ellis, "Survey of Plasma Acceleration Research," *Proceedings of the NASA-University Conference on the Science and Technology of Space Exploration*, Vol. 2, Nov. 1962, pp. 373-375.
- 6 E. C. Lary, R. G. Meyerand, F. Salz, "Ion Acceleration in a Gyro-Dominated Neutral Plasma – Theory," *Bulletin of the American Physical Society*, Ser. II., Vol 7, July 1962, p. 441.
- 7 F. Salz, R. G. Meyerand, E. C. Lary, "Ion Acceleration in a Gyro-Dominated Neutral Plasma – Experiment," *Bulletin of the American Physical Society*, Ser. II., Vol 7, July 1962, p. 441.
- 8 G. S. Janes and R. S. Lowder, "Anomalous Electron Diffusion and Ion Acceleration in a Low-Density Plasma," *The Physics of Fluids*, Vol. 9, No. 6, June 1966.
- 9 S. D. Grishin, S. D., and L. V. Leskov, *Electrical Rocket Engines of Space Vehicles*, Publishing House Mashinostroyeniye, Moscow, 1989.
- 10 A. I. Morozov, Yu. V. Esipchuk, G. N. Tilinin, A. V. Trofimov, Yu. A. Sharov, G. Ya Shchepkin, "Plasma Accelerator with Closed Electron Drift and Extended Acceleration Zone," *Soviet Physics – Technical Physics*, Vol. 17, No. 1, July, 1972.
- 11 A. I. Morozov, Yu. V. Esipchuk, A. M. Kapulkin, V. A. Nevrovskii, V. A. Smirnov, "Effect of the Magnetic Field on a Closed-Electron-Drift Accelerator," *Soviet Physics – Technical Physics*, Vol. 17, No. 3, September, 1972.
- 12 J. Brophy, J. Barnett, J. Sankovic, D. Barnhart, "Performance of the Stationary Plasma Thruster: SPT-100," AIAA-92-3155, 28th AIAA/SAE/ASME/ASEE Joint Propulsion Conference, Nashville, TN, July 6-8, 1992.
- 13 J. Szabo, "A Laboratory Scale Hall Thruster," AIAA-95-2926, 32st AIAA/ASME/SAE/ASEE Joint Propulsion Conference, San Diego, CA, July 10-12, 1995.
- 14 Busek Co. Inc., "Hall Field Plasma Accelerator with Inner and Outer Anode," U.S. Patent No. 6,075,321, 13 Jun 2000.
- 15 T. Haag, "Design of a Thrust Stand for High Power Electric Propulsion Devices," AIAA-89-2829, 25th Joint Propulsion Conference, Monterey, CA, July 10-12, 1989.
- 16 T. Haag, M. and Osborn, "RHETT/EPDM Performance Characterization," IEPC-97-107, 25th International Electric Propulsion Conference, Cleveland, OH, August 24-28, 1997.
- 17 V. Blateau, M. Martinez Sanchez, O. Batishchev, J. Szabo "PIC Simulation of High Specific Impulse Hall Effect Thruster," IEPC-01-037, 27th International Electric Propulsion Conference, Pasadena, CA, October 15-19, 2001.
- 18 Y. Azziz, "Instrument Development and Plasma Measurements on a 200-Watt Hall Thruster Plume," M.S. Thesis, Department of Aeronautics and Astronautics, Massachusetts Institute of Technology, Cambridge, MA, 2003.
- 19 Y. Azziz and M. Martinez-Sanchez, "Plasma Measurements on a 200-Watt Hall Thruster Plume," IEPC-2003-140, 28th International Electric Propulsion Conference, Toulouse, France, March 17-21, 2003.
- 20 M. Walker. Hofer, A. Gallimore, "The Effects of Nude Faraday Probe Design and Vacuum Facility Backpressure on the Measured Ion Current Density Profile of Hall Thruster Plumes," AIAA 2002-4253, 38th Joint Propulsion Conference, Indianapolis, IN, July 7-10, 2002.

-
- 21 J. Szabo, N. Warner and M. Martinez-Sanchez, "Instrumentation and Modeling of a High Isp Hall Thruster," AIAA 2002-4248, 38th Joint Propulsion Conference, Indianapolis, IN, July 7-10, 2002.
- 22 Y. Azziz, M. Martinez-Sanchez, J. Szabo, "Effect of Discharge Voltage on Plume Divergence of a High Specific Impulse Hall Thruster," AIAA-2005-4403, 41st AIAA Joint Propulsion Conference, Tucson, AZ, July 10-13, 2005.
- 23 McVey, J., Britt, E., Engelman, S., Gulczinski, F., Beiting, E. and Pollard, J., "Characteristics of the T-220HT Hall-Effect Thruster," AIAA 2003-5158, 39th Joint Propulsion Conference, Huntsville, AL, July 20-23, 2003.
- 24 J. Szabo, "Fully Kinetic Numerical Modeling of a Plasma Thruster," Ph.D. Thesis, MIT Department of Aeronautics and Astronautics, Feb 2001.
- 25 V. Khayms, M. Martinez-Sanchez, "Fifty-Wall Thruster for Microsatellites," in *Micropropulsion for Small Spacecraft*, Progress in Astronautics and Aeronautics, Vol 187, AIAA, 2000.
- 26 E. Wilson, *An Introduction to Scientific Research*, New York: McGraw Hill, 1952, pp. 272-274.